DISSERTATION

COLORADO STATE UNIV'S THESIS TEMPLATE

Submitted by

Matthew Gregory Hogan

Department of Physics

In partial fulfillment of the requirements

For the Degree of Doctor of Philosophy

Colorado State University

Fort Collins, Colorado

Summer 2019

Doctoral Committee:

Advisor: Walter Toki
Co-Advisor: Robert Wilson

Norman Buchanan
Wen Zhou

ABSTRACT

COLORADO STATE UNIV'S THESIS TEMPLATE

This document aims to get you started typesetting your thesis or dissertation in LaTeX.

ACKNOWLEDGEMENTS

I would like to thank the Elliott Forney for making a publicly accessible LaTeX template

TABLE OF CONTENTS

LIST OF TABLES

LIST OF FIGURES

Chapter 1

Introduction

Chose trop vue n'est chère tenue

A thing too much seen is little prized

French proverb

1.1 Introduction to Neutrinos

The history of the neutrino can be traced back to electron energy spectrum observed in neutron β-decay. While measurements of α- and γ-decay of atomic nuclei showed discrete spectral lines, the electron (β particle) exhibited a continuous energy spectrum. Experimentally, there were two observed particles in each decay process and classical physics dictated that the outgoing daughter particles should have discrete energies. The fact that the β-decay spectrum was not this way posed a fundamental problem for physicists in the mid-1910s and later, was energy conserved? Two solutions were postulated: either the "energy conservation law is only valid statistically in such a process [...] or an additional undetectable new particle [...] carrying away the additional energy and spin [...] is emitted [25]." The latter solution was supported by Wolfgang Pauli in a letter dated 4 December 1930 to a group of physicists meeting in Tübingen, modern Germany, where he first proposed the neutrino[1]. Pauli's solution also predicted that the undetected neutrino would have half-integer spin, a quantum mechanical property of matter, since the observed particles in β-decay did not conserve angular momentum. The existence of the neutrino and validation of Pauli's predictions would not experimentally verified for another 20 years.

The neutrino was first discovered in 1953 by Clyde Cowan and Frederick Reines using a nuclear reactor in South Carolina, U.S.A.. Since then three types of neutrinos have been observed and from unique sources like the Sun and a supernova. Neutrino physics continues to be an active region of physics since neutrinos are unique probes to processes otherwise inaccessible in laboratories. For instance in the depths of the Sun's core where fusion occurs and neutrinos are created, neutrinos are able to travel through the ultra dense and hot

[1] In W Pauli's December 1930 letter, he referred to his proposed particle as the "neutron", which is not the same neutron known of today. At that point in time, the neutral particles inside the atomic nucleus, also called "neutrons", had not been discovered, let alone understood. The neutron, which was discovered in 1932 by James Chadwick, has been formally associated as the neutral, cousin particle to the proton. It would be Enrico Fermi who would coin the particle in W Pauli's letter and solution to the β-decay spectrum as a "neutrino" meaning in Italian *little neutral one*.

medium of the core (over 10^7 degrees Kelvin) and outer layers of the Sun and reach us on Earth.

Neutrinos rarely interact with normal matter, meaning that they travel essentially unimpeded towards one's particle detector. The rarity of such interactions can be illustrated with the fact that given nearly 7.0×10^{10} neutrinos/cm^2/sec are incident on the Earth from the Sun[2], statistically one solar neutrino can harmlessly interact with an individual in her lifetime. So this begs the question: how does one detect a neutrino? The short answer is one needs a ultra large volume of matter and a large enough flux of neutrinos in its path just to detect one given today's technology.

Scientists continue to be interested in neutrinos due to properties they exhibit. One of the more recent and surprising aspects about neutrinos is their ability to undergo "flavor oscillations" where a neutrino of definite flavor (type) is created and later observed as a different flavor. The impact of such oscillations could help explain the observed matter and anti-matter asymmetry in the Universe.

1.1.1 Neutrinos in the Standard Model

The Standard Model (SM) of particle physics is the theory that describes the electromagnetic, strong nuclear, and weak nuclear forces and the elementary particles therein. These three forces and the gravitational force constitute the four *known* fundamental forces of the Universe. Each force in the SM has at least one "force carrier" particle that mediates the interactions between particles. The force carriers are formally called "gauge bosons" which indicates they are particles with integer $(0, 1, 2, ...)$ spin that come in temporary but unobservable existence to mediate the interaction. The weak nuclear bosons, the charged $W^{\pm}$ and neutral Z, couple to neutrinos as well as the other fermions, particles with half-integer

[2]To give some perspective to this number, this means 70 billion neutrinos are traveling every second through an area similar to one's own thumb nail.

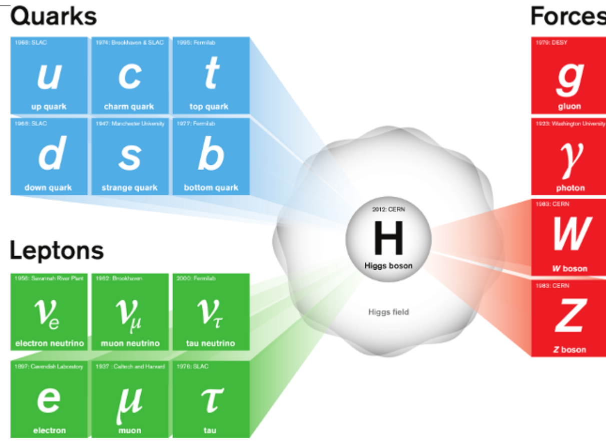

Figure 1.1: The Standard Model of particle physics consists of six quarks (up, down, strange, charm, bottom, and top), six leptons (electron, muon, tau, electron neutrino, muon neutrino, and tau neutrino), four force propagating bosons (gluon, photon, W, and Z), and the Higgs boson. The quarks, electron, muon, tau, W, and Z all gain mass through the Higgs field. The focus of this thesis are the neutrinos which are classified according to their charged, more massive Lepton cousins. Image taken from [5].

$\left(\frac{1}{2}, \frac{3}{2}, \frac{5}{2}, \ldots\right)$ spin, in the SM. All the elementary particles of the SM are shown in Figure 1.1 on page 4.

Neutrinos in the SM are electrically neutral, massless particles categorized into three generations based on their charged, more massive Lepton cousins. The neutrino and charged lepton pair into a "weak isospin doublet" in the SM. These doublets are locally gauge invariant under a SU(2)×U(1) symmetry which leads to the required existence of the photon and W and Z bosons[3].

What follows is a brief introduction to neutrino interactions as well as some of their fundamental properties.

[3]A gauge theory describes ways to measure physical forces or fields through interactions between elementary particles. The electric or magnetic fields for example can only be probed by charged particles. In the realm of quantum field theories, fields are postulated to permeate everywhere and it is excitations of these fields which produce experimental observables. Fields are constructed using the Lagrangian formalism and altered using gauge transformations. If altering the Lagrangian in some way does not affect the observables, this is referred to as a gauge invariance. Local gauge invariance means that under the constraints of the experiment, certain gauge transformations do not affect the observables. The allowed locally gauge invariant transformations require knowledge of its underlying Lie, or symmetry, group. With the weak isospin doublets, the Lie groups are SU(2)×U(1) where SU(2) is the special unitary group of 2×2 unitary matrices, and U(1) is the unitary (circle) group consisting of complex numbers of magnitude 1.

1.1.1.1 Neutrino Weak Interactions

The name "weak force" comes from the fact that this force is has a much smaller effective range than the electromagnetic, strong nuclear, and gravitational forces. This is due to the weak mediating bosons, the $W^{\pm}$ and Z, being massive particles unlike the massless gluon (g) and photon (γ). The W/Z have masses of 80/90 GeV/c^2, which is more massive than all the elementary particles except for the top quark.

For weak interactions to occur at energies far below the masses (also called "off-shell") of the W and Z, the interaction time must be infinitesimally small as dictated by the Heisenberg Uncertainty Principle

$$\Delta E \Delta t \gtrsim \hbar \tag{1.1}$$

where ΔE is the energy of the particle and Δt is the time which the particle exists. As an example, consider a neutrino of energy of 1 GeV emitting a Z-boson of off-shell energy, $\Delta E = 1$ GeV like shown in Figure 1.2 on page 6. The lifetime of that boson is about 10^{-25} seconds according to (1.1). In general, the probability that a massive particle of mass M will be created from the collision of two particles is given by a relativistic Breit–Wigner distribution

$$f(M) \propto \frac{1}{\left(\left(M^2 - M_0^2\right) c^4\right)^2 + \left(M_0 c^2 \Gamma\right)^2}, \tag{1.2}$$

where M_0 is the rest mass and Γ is the decay width of the particle in units of energy. For $M \ll M_0$, the probability of creating that particle will be infinitesimally small. Therefore to observe a single weak interaction requires a large amount of weakly interacting particles.

Weak interactions are classified into two classes of interactions: charged current (CC) and neutral current (NC). CC interactions involve a charged W boson and change the scattering neutrino into a electrically charged lepton of flavor l where the flavor of the neutrino ν_l is inferred from the charged lepton. The same cannot be said of NC interactions which exchange a neutral Z boson. NC interactions are flavor agnostic since they do not produce a charged lepton. An example of each interaction type is shown in Figure 1.2 on page 6.

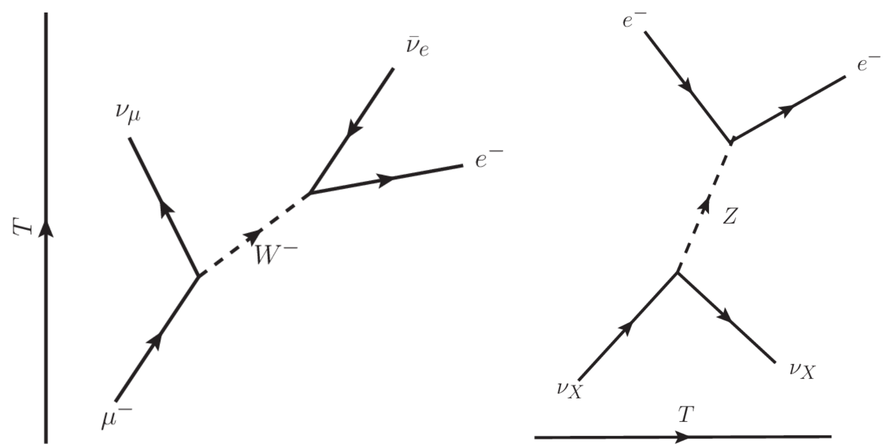

(a) Muon Decay **(b)** $\nu + e^-$ NC Scattering

Figure 1.2: (a) Muon decay $\left(\mu^- \to \nu_\mu \overline{\nu}_e e^-\right)$ Feynman diagram with time increasing from bottom to top. This is a charged current process that converts a muon into a muon neutrino via the emission of a W boson. Due to a conserved quantum number called lepton number, the W must emit an electron and electron neutrino pair. (b) Neutral current interaction Feynman diagram where time increases from left to right. This is a neutral current interaction where a neutrino of arbitrary flavor X scatters off an electron via the emission of a Z boson.

1.1.1.2 Chirality: How Neutrinos are Left Handed

Neutrinos are observed to have anti-parallel momentum vectors $\boldsymbol{P}$ to their spin vectors $\boldsymbol{\Sigma}$ and the opposite is true for anti-neutrinos. This property is called helicity and is given by (1.3)

$$\mathcal{H} = \frac{\boldsymbol{\Sigma} \cdot \boldsymbol{P}}{|\boldsymbol{P}|}. \tag{1.3}$$

While detecting neutrinos is hard as it is, the helicity is inferred from the daughter muon in charged pion decay. Since a pion has net zero (0) spin, the spin vectors of the daughters must also sum to zero. The muon from a π^+ decay has negative helicity (-1) hence the neutrino also has negative helicity. To confirm the anti-neutrino's helicity is positive (+1), the interaction requires both a charge (C) conjugation and parity (P) transformation as shown in Figure 1.3 on page 7. A C conjugation is a linear transformation that transforms all particles into their corresponding antiparticles while the P transformation inverts all spatial coordinates. Thus neutrinos are referred to *left-handed* (LH) particles while anti-neutrinos are *right-handed* (RH) particles. It turns out helicity is a useful quantum number to describe neutrinos and

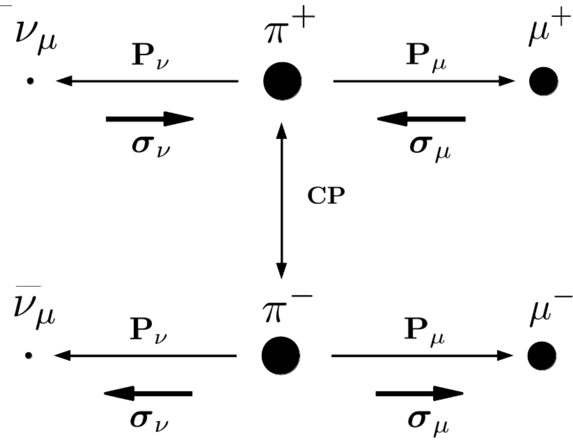

Figure 1.3: Decay of a charged pi meson into a muon and neutrino show the direction of the momentum $\boldsymbol{P}$ and spin $\boldsymbol{\sigma}$ of the outgoing particles. Since a pion at rest has zero (0) angular momentum, the system of daughter particles must have net zero angular momentum as well. A neutrino (antineutrino) is a right- (left-) handed helicity particle since its spin is (anti-)parallel to its momentum. Application of charge and parity (CP) converts all the particles into their respective antiparticles.

coincides with a property called chirality. To understand chirality and its relationship to helicity requires an analysis of the Dirac Lagrangian and Dirac equation.

The Dirac Lagrangian for a free particle field $\psi(x)$ with half-integer spin can be written as

$$\mathcal{L} = \overline{\psi}(x) \left[\frac{i\hbar}{2} \sum_{\mu=0}^{3} \gamma^\mu \left(\overrightarrow{\partial_\mu} - \overleftarrow{\partial_\mu} \right) - mc \right] \psi(x) \tag{1.4}$$

where $\psi(x)$ is a four-component vector (spinor) describing a particle field and γ^μ are a set of four 4×4 matrices. The adjoint field $\overline{\psi}(x)$ is defined as

$$\overline{\psi}(x) \equiv \psi^\dagger(x)\gamma^0 \tag{1.5}$$

where $\dagger$ denotes the conjugate and transpose operations. The $\overrightarrow{\partial_\mu}$ operator is a four-vector defined as

$$\partial_0 = \frac{1}{c}\frac{\partial}{\partial t}, \partial_1 = \frac{\partial}{\partial x}, \partial_2 = \frac{\partial}{\partial y}, \partial_3 = \frac{\partial}{\partial z} \tag{1.6}$$

that acts only on the right of it while $\overleftarrow{\partial_\mu}$ only acts on its left (i.e. $\overline{\psi}\overleftarrow{\partial_\mu} = \partial_\mu\overline{\psi}$). The γ^μ matrices are not unique and different representations dictate different kinematic regimes.

The field equations are extracted from the Lagrangian using the Euler-Lagrange procedure. In general for a set of M fields, the field equation are given by

$$\partial_\mu \frac{\partial \mathcal{L}}{\partial \left(\partial_\mu \psi_r\right)} - \frac{\partial \mathcal{L}}{\partial \psi_r} = 0 \quad (r = 0, 1, 2, \ldots, M-1, M) \,. \tag{1.7}$$

For the Dirac Lagrangian, the field equation for ψ is given by

$$\partial_\mu \frac{\partial \mathcal{L}}{\partial \left(\partial_\mu \overline{\psi}\right)} - \frac{\partial \mathcal{L}}{\partial \overline{\psi}} = 0 \tag{1.8}$$

which yields the Dirac equation

$$\left[i\hbar \sum_{\mu=0}^{3} \gamma^\mu \partial_\mu - mc\right] \psi\left(x\right) = 0. \tag{1.9}$$

The representation of the γ^μ matrices that is useful to describe neutrinos is the *Chiral representation* (also called the *Weyl representation*) where

$$\gamma^0 = \begin{bmatrix} 0 & I_2 \\ -I_2 & 0 \end{bmatrix}, \gamma^1 = \begin{bmatrix} 0 & \sigma_x \\ -\sigma_x & 0 \end{bmatrix}, \gamma^2 = \begin{bmatrix} 0 & \sigma_y \\ -\sigma_y & 0 \end{bmatrix}, \gamma^3 = \begin{bmatrix} 0 & \sigma_z \\ -\sigma_z & 0 \end{bmatrix}, \tag{1.10}$$

I_2 is the 2×2 identity matrix, $\sigma_{x,y,z}$ are the Pauli Spin matrices given by

$$\sigma_x = \sigma_1 = \begin{pmatrix} 0 & 1 \\ 1 & 0 \end{pmatrix}, \quad \sigma_y = \sigma_2 = \begin{pmatrix} 0 & -i \\ i & 0 \end{pmatrix}, \quad \sigma_z = \sigma_3 = \begin{pmatrix} 1 & 0 \\ 0 & -1 \end{pmatrix}.$$

Using the Chiral representation, the chirality matrix, γ^5 (the fifth gamma matrix), is defined as

$$\gamma^5 = i\gamma^0\gamma^1\gamma^2\gamma^3 = \begin{bmatrix} I_2 & 0 \\ 0 & -I_2 \end{bmatrix}, \tag{1.11}$$

which is diagonal as well as Hermitian meaning that its eigenvalues are real and observable. Let eigenfunctions of the chirality matrix be denoted with subscripts P and M such that the eigenvalue equations are

$$\begin{aligned} \gamma^5 \psi_P &= +1 \psi_P, \\ \gamma^5 \psi_M &= -1 \psi_M. \end{aligned} \tag{1.12}$$

The field equation solutions to (1.9) can be decomposed into ψ_P and ψ_M projections using two chiral projection operators $\hat{O}_{P,M}$ where

$$\psi = \left(\hat{O}_P + \hat{O}_M\right) \psi = \psi_P + \psi_M. \tag{1.13}$$

The chiral operators are explicitly given by

$$\begin{aligned} \hat{O}_M &= \frac{1}{2}\left(I_4 - \gamma^5\right) = \begin{pmatrix} 0 & 0 \\ 0 & I_2 \end{pmatrix}, \\ \hat{O}_P &= \frac{1}{2}\left(I_4 + \gamma^5\right) = \begin{pmatrix} I_2 & 0 \\ 0 & 0 \end{pmatrix}, \end{aligned} \tag{1.14}$$

where I_4 is the 4×4 identity matrix. Taken together (1.13) and (1.14) indicate the free neutrino field is a vector ψ minus axial vector $\gamma^5 \psi$, also referred to as V-A, under P transformations. This feature is what allows for the weak force to violate P-symmetry and CP-symmetry. Referring back to(1.4) and (1.7), the Dirac equation becomes a set of coupled equations

$$\begin{aligned} i\hbar \sum_{\mu=0}^{3} \gamma^\mu \partial_\mu \psi_P &= mc\psi_M, \\ i\hbar \sum_{\mu=0}^{3} \gamma^\mu \partial_\mu \psi_M &= mc\psi_P \end{aligned} \tag{1.15}$$

where dynamics are set by the mass.

Since the chiral projection operators are decompositions of the identity matrix, the simplest nontrivial solution to ψ is

$$\psi = \begin{pmatrix} \chi_P \\ \chi_M \end{pmatrix} \tag{1.16}$$

where χ represent two-component spinors. Using 1.16 the Dirac equation in (1.15) can again be rewritten as

$$\begin{aligned} i\hbar\left[\frac{1}{c}\frac{\partial}{\partial t}+\boldsymbol{\sigma}\cdot\boldsymbol{\nabla}\right]\chi_P &= -mc\chi_M, \\ i\hbar\left[\frac{1}{c}\frac{\partial}{\partial t}-\boldsymbol{\sigma}\cdot\boldsymbol{\nabla}\right]\chi_M &= -mc\chi_P, \end{aligned} \tag{1.17}$$

where

$$\boldsymbol{\sigma}\cdot\boldsymbol{\nabla} = \sigma_x\frac{\partial}{\partial x}+\sigma_y\frac{\partial}{\partial y}+\sigma_z\frac{\partial}{\partial z}. \tag{1.18}$$

In the limiting case of vanishing mass ($m \to 0$), as is in the SM, the free particle field equations in (1.17) decouple into

$$\begin{aligned} \left(\frac{E}{c}+\boldsymbol{\sigma}\cdot\boldsymbol{P}\right)\chi_P &= 0, \\ \left(\frac{E}{c}-\boldsymbol{\sigma}\cdot\boldsymbol{P}\right)\chi_M &= 0, \end{aligned} \tag{1.19}$$

where the differential operators have been evaluated as the particle's energy E and momentum three-vector $\boldsymbol{P}$. For massless neutrinos, χ_P and hence ψ_P, describe particles of negative energy $E = -|\boldsymbol{P}|\,c$ which in the context of quantum field theory are interpreted as antiparticles traveling backwards in time. Conversely, ψ_M have positive energy $E = |\boldsymbol{P}|\,c$ and which means they are particles traveling forward in time.

If one also multiplies (1.15) by $\gamma^5\gamma^0$ and using the fact that the spin operator $\boldsymbol{\Sigma}$ is

$$\boldsymbol{\Sigma} = i\left(\gamma^2\gamma^3,\gamma^3\gamma^1,\gamma^1\gamma^2\right) = \gamma^0\gamma^k\gamma^5 \quad (k=1,2,3) \tag{1.20}$$

each decoupled equation becomes

$$\frac{\boldsymbol{\Sigma}\cdot\boldsymbol{P}}{|\boldsymbol{P}|}\psi_{P,M} = \gamma^5\psi_{P,M} = \pm\psi_{P,M}, \tag{1.21}$$

where one recognizes that helicity and chiral states are the same for $m \to 0$ only. Thus the labels M and P actually are identical to the LH and RH helicity labels, respectively. Using the results on helicity from before, a neutrino is always observed as a LH particle while the anti-neutrino is always observed as a RH antiparticle.

The observation of only LH neutrinos and RH anti-neutrinos is an important feature in the SM. However, since neutrinos are known to have mass from oscillations, it is theoretically possible to observe a RH neutrino and LH anti-neutrino. That would require boosting to a highly relativistic reference frame with respect to the laboratory.

1.1.2 Neutrino Oscillations

Neutrino oscillations are the observation of a neutrino produced of definite flavor and later observed as a different flavor. This phenomenon was first observed as a deficit of neutrinos for a number of atmospheric and solar neutrino experiments. The deficit also seemed more pronounced for atmospheric neutrinos as the distance from their source increased. For neutrino oscillations to occur, at least one neutrino must be massive. This observation firmly established that the SM is wrong with its prediction of massless neutrinos.

The first indication of neutrino oscillations was from the Ray Davis Homesteak Mine experiment which began in the 1960s. Ray Davis was an expert Chemist and designed a radiochemical experiment to measure the flux of neutrinos from Sun. The purpose of this experiment was to test John Bahcall's prediction of the fusion rate in the Sun and neutrino flux from it as well. Davis' experiment would need to operate for many years to collect enough statistics due to expected low capture rate. Measurements continued into the 1980s and showed that the flux of neutrinos as measured at Homesteak was about 1/3 the expected rate and became known as the "Solar Neutrino Problem." The primary solutions were either the the solar model was incorrect or the neutrino capture cross section is incorrect somehow. The Sudbury Neutrino Observatory (SNO) was able to resolve this problem by making a model-independent measurement of the solar neutrino flux. SNO observed a ν_eCC-to-NC ratio of 0.301 ± 0.033, which confirmed that only about 30% of neutrinos arrive as ν_e flavors on Earth. Saying this another way, the majority of neutrinos arrive as the wrong flavor [25].

Another outstanding problem emerged with measurements of atmospheric neutrinos, in particular muon and electron types. Atmospheric neutrinos are produced when high energy cosmic rays strike atmospheric particles. These cosmic ray collisions generate mostly pions and kaons that decay into neutrinos. When trying to measure the ν_μ/ν_e ratio and comparing that with expected ratio, there was another significant deficit. This was particularly a problem as a function of the zenith angle for the Super-Kamiokande (SK) experiment. SK is a 50kt tank of pure water lined with thousands of photomultiplier tubes designed to observe solar and atmospheric neutrinos. It was the first experiment to perform a neutrino oscillation analysis that successfully explained the deficit.

While the phenomenon of neutrino oscillations has been understood for almost three decades, it was not predicted since oscillations require the neutrino has mass. The reasons why neutrino oscillations require massive neutrinos are explained in the next subsection.

1.1.2.1 Two Flavor Derivation

The phenomenon of neutrino oscillations can be described with elementary, non-relativistic Quantum Mechanics. Beginning with the Schrödinger Equation in (1.22)

$$-\frac{\hbar}{i}\frac{d}{dt}\left|\nu(\mathbf{r},t)\right\rangle = \hat{H}\left|\nu(\mathbf{r},t)\right\rangle, \tag{1.22}$$

where $\hat{H}$ is the Hamiltonian for the physical system, one considers a massive neutrino of mass m_j in its rest frame (free particle). The Hamiltonian is diagonal in this case, which acting on $\left|\nu_j\right\rangle$ results in the eigenvalue equation

$$\hat{H}\left|\nu_j(\mathbf{r},t)\right\rangle = E_j\left|\nu_j(\mathbf{r},t)\right\rangle, \tag{1.23}$$

where E_j is the energy of the neutrino $\left|\nu_j\right\rangle$. Substituting (1.23) into (1.22) and solving for $\left|\nu(\mathbf{r},t)\right\rangle$, one obtains the following

$$\left|\nu_j(\mathbf{r}, t)\right\rangle = e^{-iE_jt/\hbar}\left|\nu_j(\mathbf{r}, t=0)\right\rangle, \tag{1.24}$$

where $\left|\nu_j(\mathbf{r}, t=0)\right\rangle$ is created with momentum $\mathbf{p}$ at the origin $\mathbf{r} = 0$. The time-independent solution to (1.22) is a plane-wave given by

$$\left|\nu_j(\mathbf{r}, t=0)\right\rangle = e^{i\mathbf{p}\cdot\mathbf{r}/\hbar}\left|\nu_j\right\rangle. \tag{1.25}$$

Before being able to describe neutrino oscillations, the basis states must be defined. For this example, consider that there are only two eigenstates, labeled ν_1 and ν_2, in the "mass" basis with definite mass m_1 and m_2, respectively. However, experiments can produce neutrinos, as well as probe them, only of definite "flavor", denoted by a Greek letter subscript λ. Let the generated neutrino, which is a linear superposition of mass states 1 and 2, have momentum $\mathbf{p}$ and flavor α. Since both mass eigenstates share the same momentum momentum $\mathbf{p}$ (but not energy!), the exponential term in (1.25) is an overall phase that will cancel out later. One can postulate a linear transformation, U, between the basis states given by (1.26).

$$\begin{bmatrix} \nu_\alpha \\ \nu_\beta \end{bmatrix} = \begin{bmatrix} U_{11} & U_{12} \\ U_{21} & U_{22} \end{bmatrix} \begin{bmatrix} \nu_1 \\ \nu_2 \end{bmatrix} \tag{1.26}$$

This linear transformation must be a unitary matrix $\left(U^{-1} = U^\dagger, \dagger = \text{transpose conjugate}\right)$ since the states $\nu_{1,2}$ constitute a complete orthonormal basis in the mass basis. With this unitary property, U can be written as a rotation matrix

$$\begin{bmatrix} \nu_\alpha \\ \nu_\beta \end{bmatrix} = \begin{bmatrix} \cos(\theta) & \sin(\theta) \\ -\sin(\theta) & \cos(\theta) \end{bmatrix} \begin{bmatrix} \nu_1 \\ \nu_2 \end{bmatrix}, \tag{1.27}$$

where θ is the angle between the two bases. One can imagine this transformation between bases as shown in Figure 1.4 on page 14 . Creating a neutrino of flavor α and observe it after a time $t = T > 0$, the probability of observing it as flavor $\beta \neq \alpha$ is given by

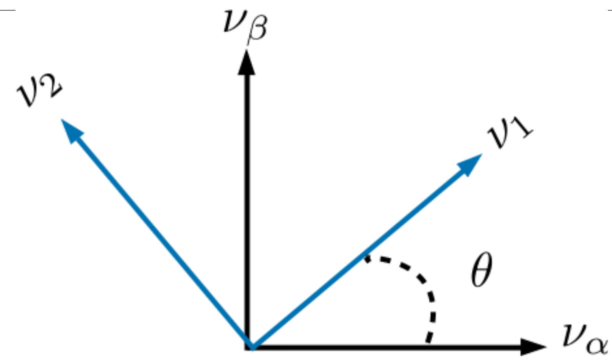

Figure 1.4: The depiction of two neutrino flavor change of basis using a rotation matrix. Compare this with (1.27).

$$\begin{aligned} \mathcal{P}\left(\nu_\alpha \to \nu_\beta\right) &= \left|\langle \nu_\alpha(t=0)|\nu_\beta(t=T)\rangle\right|^2 \\ &= |(\cos(\theta)\,\langle \nu_1(t=0)| + \sin(\theta)\,\langle \nu_2(t=0)|) \\ &\times\,(-\sin(\theta)\,|\nu_1(t=T)\rangle + \cos(\theta)\,|\nu_2(t=T)\rangle)|^2 . \end{aligned} \tag{1.28}$$

Evaluating all inner products and simplifying terms in (1.28) results in (1.29) below.

$$\mathcal{P}\left(\nu_\alpha \to \nu_\beta\right) = \sin^2(2\theta)\sin^2\left(\frac{E_1 - E_2}{2\hbar}T\right) \tag{1.29}$$

The terminology of "neutrino oscillations" should be more apparent now since (1.29) demonstrates that the probability changes sinusoidally. This equation is not, however, terribly useful in the laboratory frame since it is hard to design an experiment where the travel time an individual neutrino is well known. Instead, one can make useful approximations that are accessible in the laboratory frame. Since neutrinos are nearly massless, they travel very close to the speed of light. Therefore time T is replaced with L/c where L is the distance between the neutrino origin and detection and c is now the speed of light in vacuum. One can also approximate the energy of the mass eigenstate as

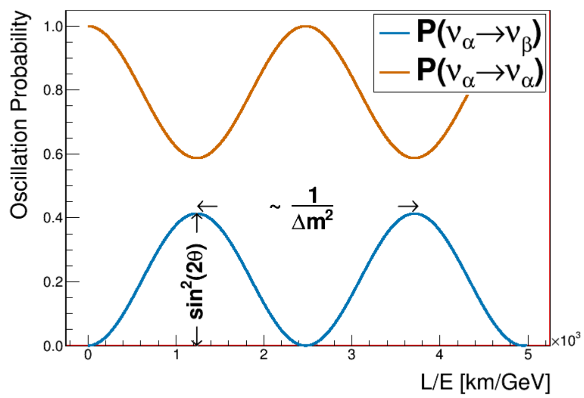

Figure 1.5: Two flavor oscillation probability as a function L/E is shown using $\theta = 20^\circ$ and $\Delta m^2 = 10^{-3}$ eV$^2/c^4$. The spacing between adjacent peaks/troughs is proportional to the inverse of Δm^2. Note that $\mathcal{P}(\nu_\alpha \to \nu_\alpha) = 1 - \mathcal{P}(\nu_\alpha \to \nu_\beta)$ since the oscillation probability must always sum to 1.

$$
\begin{aligned}
E_j = \left(m_j^2 c^4 + p_j^2 c^2\right)^{\frac{1}{2}} &= p_j c \left(1 + \frac{m_j^2 c^2}{p_j^2}\right)^{\frac{1}{2}} \\
&\approx p_j c \left(1 + \frac{m_j^2 c^2}{2p_j^2} + \mathcal{O}\left(\frac{m_j c}{p_j}\right)^4\right) \\
&\approx E_\nu + \frac{m_j^2 c^4}{2E_\nu},
\end{aligned}
\tag{1.30}
$$

where for oscillation experiments $p_j \gg m_j c$ and $p_j c \approx E_\nu$ where E_ν is the neutrino energy as measured in the laboratory. Substituting these assumptions in (1.29), the oscillation probability is given by

$$
\mathcal{P}\left(\nu_\alpha \to \nu_\beta\right) = \sin^2(2\theta) \sin^2\left(\frac{\Delta m^2 c^3}{4\hbar} \frac{L}{E_\nu}\right), \tag{1.31}
$$

where $\Delta m^2 = m_2^2 - m_1^2$ is the mass-squared difference between the mass states. For a momentum consider evaluating all the physical constants in natural units ($c = \hbar = 1$). An appropriate choice of units for Δm^2, L, and E_ν results in

$$
\mathcal{P}\left(\nu_\alpha \to \nu_\beta\right) = \sin^2(2\theta) \sin^2\left(1.27 \frac{\Delta m^2}{\left[\mathrm{eV}^2\right]} \frac{L/E_\nu}{\left[\mathrm{km}/\mathrm{GeV}\right]}\right) \quad \text{[natural units]} \tag{1.32}
$$

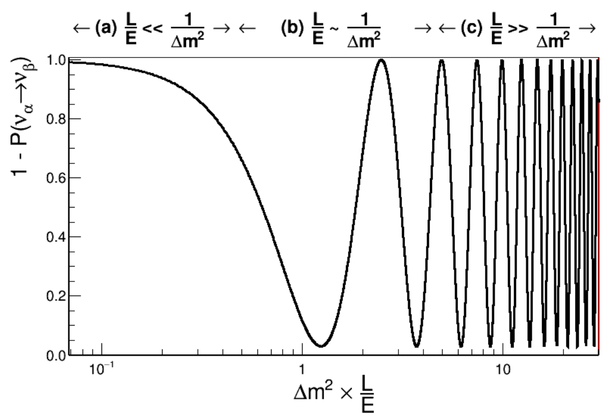

Figure 1.6: Logarithmic plot of the survival probability of flavor α $(1 - \mathcal{P}(\nu_\alpha \to \nu_\beta) = \mathcal{P}(\nu_\alpha \to \nu_\alpha))$ over a wide range of L/E values for $\theta = 40^\circ$. The arrows above the plot very roughly denote three possible cases: (a) no oscillations ($L/E \ll 1/\Delta m^2$); (b) sensitivity to oscillations ($L/E \sim 1/\Delta m^2$); (c) only average measurement ($L/E \gg 1/\Delta m^2$). Image originally inspired by [20].

which more clearly demonstrates the Physics in neutrino oscillations. The oscillation probability has an amplitude of $\sin^2(2\theta)$ and varies with frequency inversely proportional to Δm^2 as illustrated in Figure 1.5 on page 15. Since L and E_ν are the only controllable parameters for an oscillation experiment, probing θ or Δm^2 can be difficult unless the experiment can probe a large range of L/E_ν as shown in Figure 1.6 on page 16.

1.1.2.2 Three Flavor Oscillations

In the general case of oscillations using a $n \times n$ mixing matrix, the unitary transformation can be written as a rotation matrix with $\frac{n}{2}(n-1)$ weak mixing angles with $\frac{1}{2}(n-2)(n-1)$ Charge-Parity (CP) violating phases. In addition, oscillations are dictated by a total of $n-1$ mass-squared splittings [25]. This all assumes that neutrinos obey the Dirac Equation, or that they are not their own antiparticles. The favored mixing model is the 3×3 matrix since there are three known neutrino flavors, ν_e, ν_μ, and ν_τ. This means that there are three (3) mixing angles, one (1) CP violating phase, and three (3) mass-squared splittings.

The most frequently used matrix parameterization is the MNSP (MNSP: Maki-Nakagawa-Sakata-Pontecorvo) matrix. Pontecorvo is accredited for first conceiving of neutrino oscilla-

Source	Species	Baseline [km]	Mean Energy [GeV]	$\min\left(\Delta m^2\right)$ $\left[\mathrm{eV}^2\right]$
Reactor	$\overline{\nu}_e$	1	$\sim 10^{-3}$	$\sim 10^{-3}$
Reactor	$\overline{\nu}_e$	100	$\sim 10^{-3}$	$\sim 10^{-5}$
Accelerator	$\nu_\mu, \overline{\nu}_\mu$	1	~ 1	~ 1
Accelerator	$\nu_\mu, \overline{\nu}_\mu$	10^3	~ 1	$\sim 10^{-3}$
Atmospheric ν's	$\nu_{e,\mu}, \overline{\nu}_{\mu,e}$	10^4	~ 1	$\sim 10^{-4}$
Sun	ν_e	1.5×10^8	$\sim 10^{-3}$	$\sim 10^{-11}$

Table 1.1: Sensitivity of different oscillation experiments originally published in [22].

tions, albeit between neutrino and anti-neutrinos [17]. It was Maki, Nakagawa, and Sakata who conceived of the parameterization based off the ideas of Pontecorvo [16]. The MNSP matrix is decomposed into separate rotation matrices as given by (1.33)

$$U_{\mathrm{MNSP}} = \overbrace{\begin{bmatrix} 1 & 0 & 0 \\ 0 & c_{32} & s_{32} \\ 0 & -s_{32} & c_{32} \end{bmatrix}}^{U_{\mathrm{atm}}} \times \overbrace{\begin{bmatrix} c_{31} & 0 & s_{31}e^{i\delta_{\mathrm{CP}}} \\ 0 & 1 & 0 \\ -s_{31}e^{-i\delta_{\mathrm{CP}}} & 0 & c_{31} \end{bmatrix}}^{U_{\mathrm{rea}}} \times \overbrace{\begin{bmatrix} c_{21} & s_{21} & 0 \\ -s_{21} & c_{21} & 0 \\ 0 & 0 & 1 \end{bmatrix}}^{U_{\mathrm{sol}}} , \qquad (1.33)$$

where

$$c_{ij} = \cos\theta_{ij}, \quad s_{ij} = \sin\theta_{ij}, \qquad (1.34)$$

and δ_{CP} represents the CP violating phase. Each rotation matrix represents the different sources for neutrino oscillations experiments with "atm", "rea", and "sol" representing atmospheric ν's, nuclear reactor ν's, and Solar ν's, respectively. The sensitivity of neutrino oscillations for different sources is given in Table 1.1 on page 17.

If neutrinos are their own antiparticles, they do not follow the Dirac Equation but do follow the Majorana Equation. This adds two (in general $n-1$) more CP violating Majorana phases, α and β, to the MNSP matrix

$$U_{\mathrm{MNSP}} \to U_{\mathrm{MNSP}} \times \overbrace{\begin{bmatrix} 1 & 0 & 0 \\ 0 & e^{i\alpha} & 0 \\ 0 & 0 & e^{i\beta} \end{bmatrix}}^{U_{\mathrm{Majorana}}}. \tag{1.35}$$

Unfortunately, neutrino oscillations are not able to probe the Majorana phases since the Majorana matrix is diagonal. The question of if neutrinos are Majorana ($\nu = \overline{\nu}$) or Dirac ($\nu \neq \overline{\nu}$) particles is an open question and is being explored by non-oscillation experiments.

The full three flavor oscillation probability is given by

$$\begin{aligned} \mathcal{P}\left(\nu_\alpha \to \nu_\beta\right) = \delta_{\alpha\beta} - 4\sum_{j=1}^{3}\left[\sum_{i>j}^{3} \mathrm{Re}\left(K_{\alpha\beta,ij}\right)\sin^2\left(\phi_{ij}\right)\right] \\ +4\sum_{j=1}^{3}\left[\sum_{i>j}^{3} \mathrm{Im}\left(K_{\alpha\beta,ij}\right)\sin\left(\phi_{ij}\right)\cos\left(\phi_{ij}\right)\right] \end{aligned} \tag{1.36}$$

where

$$K_{\alpha\beta,ij} = U_{\alpha i}U^*_{\beta_i}U^*_{\alpha j}U_{\beta j} \tag{1.37}$$

encapsulates the MNSP matrix elements and

$$\phi_{ij} = \frac{\Delta m^2_{ij}c^3}{4\hbar}\frac{L}{E_\nu}. \tag{1.38}$$

Since CP violation means that $\mathcal{P}\left(\nu_\alpha \to \nu_{\beta\neq\alpha}\right) \neq \mathcal{P}\left(\overline{\nu}_\alpha \to \overline{\nu}_{\beta\neq\alpha}\right)$, CP violating terms must be an odd function of δ_{CP}. Consider the following examples, muon neutrino survival and muon neutrino to electron neutrino appearance.

1.1.2.2.1 Muon Neutrino Survival

The probability of a muon type neutrinos surviving is given by

$$\begin{aligned} \mathcal{P}\left(\overset{(-)}{\nu}_\mu \to \overset{(-)}{\nu}_\mu\right) = 1 - 4s^2_{23}c^2_{13}\left(V_{\cos\delta_{\mathrm{CP}}}\right)\sin^2\phi_{31} \\ -4s^2_{23}c^2_{13}\left(Z_{\cos\delta_{\mathrm{CP}}}\right)\sin^2\phi_{32} \\ -4\left(V_{\cos\delta_{\mathrm{CP}}}\right)\left(Z_{\cos\delta_{\mathrm{CP}}}\right)\sin^2\phi_{21} \end{aligned} \tag{1.39}$$

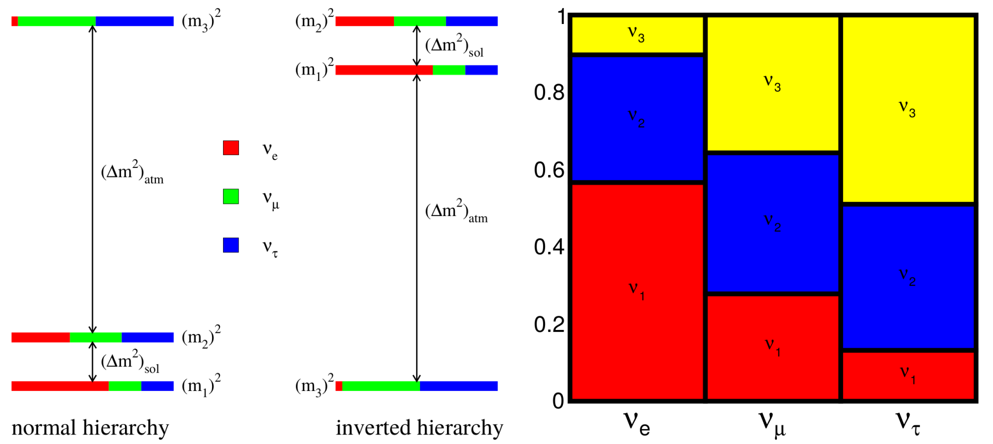

(a) Mass hierarchy as shown in [9]

(b) Mass eigenstate components as shown in [5]

Figure 1.7: Left: the mass hierarchy problem is such that while the solar and atmospheric mixing mass-squared differences are clearly defined, the absolute mass scale is unknown. Since $m_2 > m_1$ by definition, it is currently unknown if m_3 is more or less massive than m_2, or even massless! Notice the colored bars for each mass eigenstate which corresponded to the approximate flavor content of the neutrino. For example, state "2" has about equal three portions of all three flavors. Right: the mass eigenstate components of each flavor eigenstate. This is a complementary demonstration of the MNSP matrix.

where

$$V_{\cos\delta_{\mathrm{CP}}} = s_{12}^2 c_{23}^2 + s_{13}^2 s_{23}^2 c_{12}^2 + 2 s_{12} s_{13} s_{23} c_{12} c_{23} \cos\delta_{\mathrm{CP}} \tag{1.40}$$

$$Z_{\cos\delta_{\mathrm{CP}}} = c_{12}^2 c_{23}^2 + s_{13}^2 s_{23}^2 s_{12}^2 - 2 s_{12} s_{13} s_{23} c_{12} c_{23} \cos\delta_{\mathrm{CP}} \tag{1.41}$$

and $\overset{(-)}{\nu}_\mu$ represents either ν_μ or $\overline{\nu}_\mu$. Since all CP violating terms in (1.39) are even functions of δ_{CP}, this channel does not offer insights into CP violation in a vacuum[4].

1.1.2.2.2 Electron Neutrino Appearance While CP violation is not observable in muon neutrino disappearance, it is with electron neutrino appearance. The appearance probability of electron neutrinos types from muon types is given by

[4]When going to through matter however, the oscillation probability is affected. This is explained more in Section 1.1.2.3.

$$
\begin{aligned}
\mathcal{P}\left(\overset{(-)}{\nu}_\mu \rightarrow \overset{(-)}{\nu}_e\right) =& 4c_{13}^2 s_{13}^2 s_{23}^2 \sin^2\phi_{31} \\
&+ 8\left(X_{\cos\delta_{\mathrm{CP}}}\right)\cos\phi_{23}\sin\phi_{31}\sin\phi_{21} \\
&\overset{(+)}{-} 8\underbrace{\left(Y_{\sin\delta_{\mathrm{CP}}}\right)}_{\text{CP violating}}\sin\phi_{32}\sin\phi_{31}\sin\phi_{21} \\
&+ 4\left(Z_{\cos\delta_{\mathrm{CP}}}\right)s_{12}^2 c_{13}^2\sin^2\phi_{21}
\end{aligned}
\tag{1.42}
$$

where

$$X_{\cos\delta_{\mathrm{CP}}} = c_{13}^2 s_{12}s_{13}s_{23}\left(c_{12}c_{23}\cos\delta_{\mathrm{CP}} - s_{12}s_{13}\right) \tag{1.43}$$

$$Y_{\sin\delta_{\mathrm{CP}}} = \frac{1}{8}\sin\left(2\theta_{12}\right)\sin\left(2\theta_{13}\right)\sin\left(2\theta_{23}\right)c_{13}\sin\delta_{\mathrm{CP}} \tag{1.44}$$

and (+) represents the sign change from neutrinos to anti-neutrinos. The CP violating term (1.44) is also known as the Jarlskog Invariant and is a measure of CP violation independent of the mixing parameterization [14]. This oscillation channel are of primary importance in accelerator and atmospheric neutrino oscillation experiments.

Current and next generation experiments aim to improve knowledge of the mixing parameters. There are a couple of degeneracies to unravel as well as precise measurement of δ_{CP}. While the two defined mass-squared splittings $\Delta m_{21}^2 = \Delta m_{\mathrm{sol}}^2$ and $\Delta m_{32}^2 = \Delta m_{\mathrm{atm}}^2$ are known, it is unknown which eigenstates are more massive. This problem is known as the mass hierarchy problem and is illustrated in Figure 1.7a on page 19. Normal hierarchy refers to the case where $m_3 > m_2 > m_1$whereas the inverted hierarchy has $m_2 > m_1 > m_3$. Also knowledge if θ_{23} is in the first octant $\theta \in (0, \pi/2)$ or second octant $\theta \in (\pi/2, \pi/4)$ requires large statistics. Finally the value of δ_{CP} is quite uncertain with values in the 3rd and 4th quadrants. Best fit measurements of the oscillations parameters is given in Table 1.2 on page 21.

Parameter	Normal Hierarchy value	Inverted Hierarchy value	Units
$\Delta m^2_{32} = \Delta m^2_{\mathrm{atm}}$	2.51 ± 0.05	-2.56 ± 0.04	10^{-3} eV^2
$\Delta m^2_{21} = \Delta m^2_{\mathrm{sol}}$	7.53 ± 0.18		10^{-5} eV^2
$\sin^2(\theta_{21})$=$\sin^2(\theta_{\mathrm{sol}})$	$0.307^{+0.013}_{-0.012}$		1
$\sin^2(\theta_{32})$=$\sin^2(\theta_{\mathrm{atm}})$	O1: $0.417^{+0.025}_{-0.028}$ O2: $0.597^{+0.024}_{-0.030}$	O1: $0.421^{+0.033}_{-0.025}$ O2: $0.592^{+0.023}_{-0.030}$	1
$\sin^2(\theta_{31})$	2.12 ± 0.08		10^{-2}
δ_{CP}	217^{+40}_{-28}	280^{+25}_{-28}	degrees

Table 1.2: Table of best fit MNSP parameters split by normal and inverted hierarchy. O1 and O2 correspond to the first octant ($\theta \in (0, \pi/2)$) or second octant ($\theta \in (\pi/2, \pi/4)$). All values except for δ_{CP} are combined values from the Particle Data Group and δ_{CP} is from the 2018 NuFit analysis [10,22].

1.1.2.3 Matter Effects

Traveling through matter has the potential to increase the sensitivity of oscillation measurements if the baseline is long enough. Known as the Mikheyev-Smirnov-Wolfenstein (MSW) effect, all oscillations are affected by coherent forward scattering of neutrinos with electrons in the media. Taking the example of $\overset{(-)}{\nu}_\mu \rightarrow \overset{(-)}{\nu}_e$ from (1.39), the MSW effect to first order is

$$\mathcal{P}\left(\overset{(-)}{\nu}_\mu \rightarrow \overset{(-)}{\nu}_e\right) \rightarrow \mathcal{P}\left(\overset{(-)}{\nu}_\mu \rightarrow \overset{(-)}{\nu}_e\right) + \frac{8\alpha}{\Delta m^2_{31}}\left(c^2_{13}s^2_{13}s^2_{23}\right)\left(1-2s^2_{13}\right) \times \left(\sin^2\phi_{31} \overset{(+)}{-} \underbrace{\left(\frac{\Delta m^2_{31}c^3}{4\hbar}\frac{L}{E_\nu}\right)}_{\phi_{31}} \cos\phi_{32}\sin\phi_{31}\right), \tag{1.45}$$

where

$$\alpha = 2\sqrt{2}G_F n_e E_\nu \tag{1.46}$$

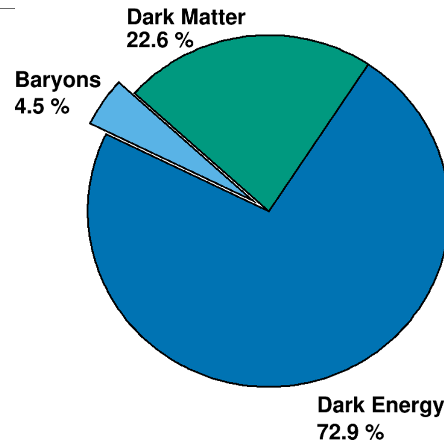

Figure 1.8: Matter and energy content of the Universe display that while the Universe consists of 4.5% of baryonic matter. The rest of the Universe consists of non-baryonic matter called Dark Matter and a form of energy called Dark Energy. These inferred parameters are taken from the ΛCDM model, the simplest model that describes the cosmos [15].

and G_F is the Fermi constant and n_e is the average electron density of the Earth which the neutrinos travel [6]. Carefully studying (1.45) reveals that the MSW effect alters the oscillation probability as a function of the electron density and increases in magnitude with baseline.

1.1.3 CP Violation: Origins of Matter

To conclude the introduction on neutrinos, it is important to examine the implications of CP violation. The observation of CP violation in the lepton sector might provide critical insight into the origins of the matter. CP violation dictates that certain interactions behave differently between matter or antimatter like $\mathcal{P}\left(\nu_\mu \to \nu_e\right) \neq \mathcal{P}\left(\overline{\nu}_\mu \to \overline{\nu}_e\right)$. The Big Bang Theory suggests that in the first fractions of a second of the Universe, equal amounts of matter and antimatter were created. However, observational evidence shows the Universe consists of only 4.5% baryonic matter (i.e. protons and neutrons) from cosmological models as shown in Figure 1.8 on page 22. The anti-baryonic fraction of the baryonic matter is infinitesimally low from external constraints on data from gamma-ray telescopes like Fermi-GLAST [23]. This problem is known as the Baryon Asymmetry of the Universe (BAU).

The process of Baryogenesis[5] is a favored model to explain the BAU and lacks a necessary precursor mechanism. One of the necessary conditions for Baryogenesis [19] is C symmetry violation and CP violation. Evidence of CP violation has been experimentally confirmed in the quarks, but not to the level which resolves the BAU. Baryogenesis can be achieved by having Leptogenesis[6] occur first through the decay of very heavy, right handed Majorana neutrino ($\nu = \overline{\nu}$) through the *see-saw* mechanism. Detailed discussions on Leptogenesis and the *see-saw* mechanism can found in [5].

1.2 Tokai-to-Kamioka Experiment

The Tokai-to-Kamioka (T2K) experiment is a long baseline, neutrino oscillation experiment hosted in Japan [1] as shown in Figure 1.9 on page 24. It is the successor experiment to the KEK-to-Kamioka neutrino oscillation experiment also hosted in Japan. T2K produces its high intensity, muon neutrino pure beam at the Japan Proton Accelerator Complex (J-PARC), a world class particle accelerator facility. The beam is directed at the Super-Kamiokande (SK) [12] detector which is 295 km away from the source. Along the beamline at 280m from the beam source are a series of near detectors called ND280 [11] to observe and characterize the unoscillated beam. The beam is designed to maximize the $\nu_\mu \to \nu_e$ probability at the L =295 km baseline using a neutrino energy spectrum sharply peaked at $E_\nu = 0.6$ GeV. This spectrum is achieved by directing the center of the beam axis 2.5 degrees off center from SK.

T2K was primarily designed to measure the last unknown MNSP mixing angle θ_{13}, which was thought to be nearly zero. In addition it set out to measure to high precision the atmospheric mixing parameters, θ_{23} and Δm^2_{23}. One of its early successes was a landmark

[5] Baryogenesis is the mechanism by which matter and antimatter baryons are created in the early Universe.

[6] Leptogenesis is the mechanism by which leptons and anti-leptons are created in the early Universe.

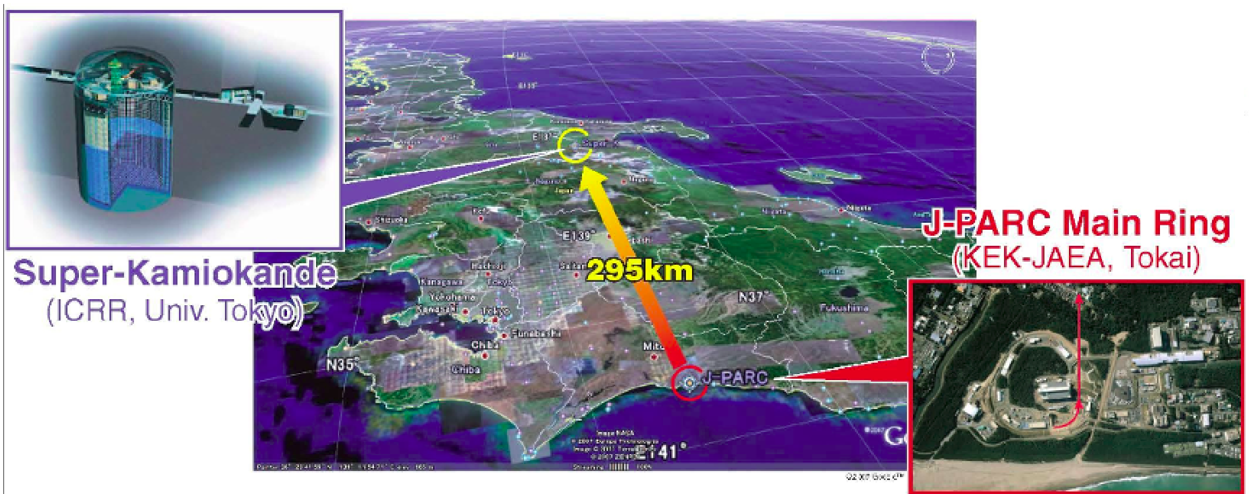

Figure 1.9: Birds eye view of the T2K experiment on the Japanese archipelago. An intense beam of neutrinos are produced at the J-PARC site (bottom right red box) using high energy protons. The beam is directed towards the Super-Kamiokande detector (top left blue box) at a distance of 295 km away from J-PARC.

7.3σ measurement of a non-zero θ_{13} using the electron-neutrino appearance measurement [3]. It continues to be a world leader in oscillation physics and as of 2018 rejects CP conserving values ($\delta_{\text{CP}} = 0, \pi$) at the 2σ level [4].

The following topics will be discussed in the following order. First a look how neutrinos are produced at J-PARC. Next a detailed look at the T2K near detectors which are used in this thesis. This is followed by a discussion on Super-Kamiokande, the T2K far detector. The final topic is the basics of an oscillation analysis using a near and far detector.

1.2.1 Neutrino Production at J-PARC

To facilitate the high intensity neutrino beam requirements for T2K, the J-PARC site generates a high intensity proton beam through a series of particle accelerators. A bird's eye view of J-PARC can be seen in Figure 1.10 on page 25 which highlights its different accelerators and facilities. For this section, note that all beam energies are kinetic energies.

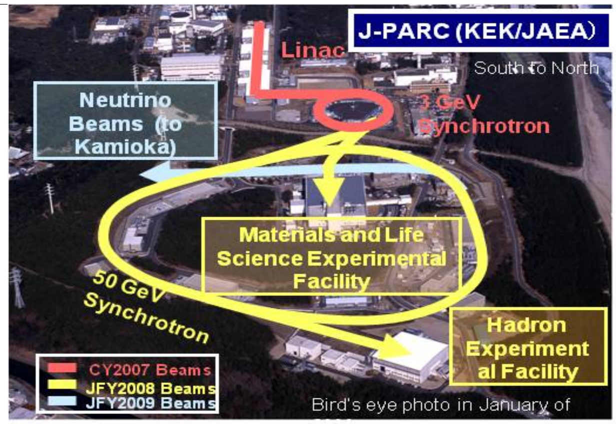

Figure 1.10: Bird's eye view of the J-PARC center showing the primary components of its accelerator programs. To generate the high intensity neutrino beam, first the linear accelerator (Linac, red) accelerates hydrogen ions (protons) into the 3 GeV Synchrotron (also red) called the rapid-cycle synchrotron (RCS). The RCS then injects some of its protons into the 50 GeV Synchrotron (yellow) called the main ring (MR) which currently runs at 30 GeV. Finally the MR protons are directed into a target material along the neutrino beamline (teal) [7].

Protons for the T2K beamline are first accelerated in the J-PARC linear accelerator[7] (linac) and then the rapid cycle synchrotron[8] (RCS). Hydrogen ions ($^1_1\mathrm{H}^-$) are extracted from plasma in a electrical discharge chamber and feed through a series of linac elements as shown in Figure 1.11a on page 26. Each linac element except for the initial quadrapole magnet apparatus accelerates the ions using carefully coordinated oscillating electric fields generated by radio frequency pulses. After traveling 240m along the linac, the ions have been boosted to 181 MeV of kinetic energy and transported into the RCS. In transit to the RCS, the ions are stripped of their electrons via charge stripping foils. The 348m circumference RCS then further boosts the protons to 3 GeV at an operating frequency of 25 Hz. While being accelerated, protons are aggregated into two bunches and focused using particle collimators as shown in Figure 1.11b on page 26.

[7] A linear accelerator accelerates particles using time varying electric fields along a one direction, terminal beamline. Not only used in particle physics, they are also used in the medical field to generate X-rays.

[8] A synchrotron is cyclic particle accelerator that relies on time varying magnetic fields to accelerate particles. Since they require many magnets and large spaces to operate, they are usually operated at national laboratories for others uses as well like material and life sciences.

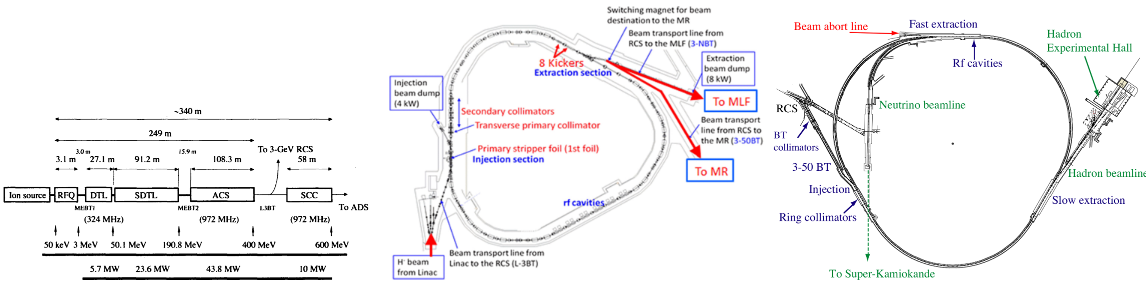

(a) 400 MeV linac **(b)** 3 GeV RCS **(c)** 50 GeV MR

Figure 1.11: Schematics of the J-PARC accelerators. (a) The linac accelerates hydrogen ions to 181 MeV of kinetic energy, designed for 400 MeV, from the ion source through linear accelerator (linac) elements [24]. (b) Protons from the linac are collected into the rapid cycle synchrotron (RCS) and accelerated to 3 GeV [18]. (c) Protons from the RCS are injected into the main ring (MR) synchrotron which further accelerates the protons. While the MR is designed for 50 GeV, it currently operates at 30 GeV. For T2K, the protons are bunched in the MR and extracted into the "Neutrino beamline" [13].

The next stage for the protons intended for the neutrino beamline is the much larger main ring (MR) synchrotron as shown in Figure 1.11c on page 26 which has a circumference of 1567m. While nominally designed to boost protons to 50 GeV, it currently operates at 30 GeV. Protons are injected into the MR to form eight proton bunches (spill), initially six when T2K first ran, before entering the neutrino beamline. The total temporal width of the spill is approximately 0.5μs [1]. At a spill cycle frequency of 0.5Hz, the bunches are extracted from the MR into the neutrino beamline.

The neutrino beamline is designed to direct the protons toward SK and generate neutrinos by impinging them on a cylindrical target. Figure 1.12a on page 27 shows the process of proton extraction from the MR for both primary and secondary neutrino beamlines. In the primary beamline, a series of normal and superconducting magnets steer the proton beam away from the MR first along a 54m preparation section and then a 147m arc section to bend the beam towards SK. A final focusing section in the primary beamline focuses the protons into the secondary beam while directing it downwards 3.637° with respect to the local horizontal. Since a well tuned and stable proton beam is necessary for neutrino production, numerous beam monitors are installed along the primary beamline to measure any losses.

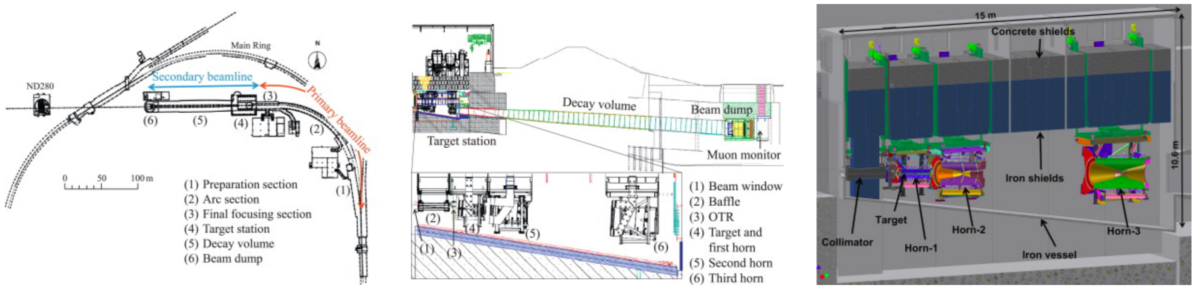

(a) Neutrino beamline **(b)** Secondary beamline **(c)** Beamline horns

Figure 1.12: The neutrino beamline at J-PARC consists of a primary and secondary beamline. (a) The primary beamline redirects the protons towards the secondary beamline [1]. (b) In the secondary beamline, the protons are impinged on a cylindrical target producing mostly pions. The pions are focused using in sequence horns and decay in a long decay volume. Any non-decayed particles are stopped at the beam dump. (c) A further zoomed in cross section of the target station showing the target and focusing horns [21].

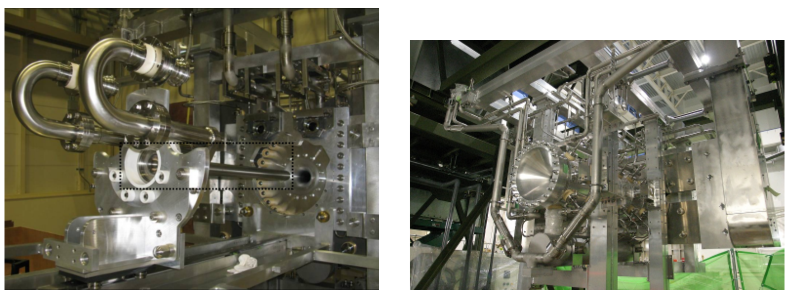

(a) A graphite target being extracted from the target station **(b)** A magnetic focusing horn

Figure 1.13: Shown are photos of work performed on the target station. (a) The graphite rod being extracted from the target station is shown in the black-dashed box. (b) One focusing horn in T2K.

The secondary beamline marks the end of the proton beam and production of a neutrino beam. In the secondary beamline, as shown in Figure 1.12b on page 27, it consists of a target station, a decay volume for the outgoing particles from the target station, and a beam dump for any remaining particles. The target station houses a 91.4cm long, 2.6cm diameter, and 1.8g/cm^3 graphite rod which corresponds to 1.9 radiation lengths. When the protons impinge the target, strong (nuclear) interactions produce pi-mesons (pions) and ka-mesons (kaons). like those produced from cosmic ray collisions in the upper atmosphere. To enhance the

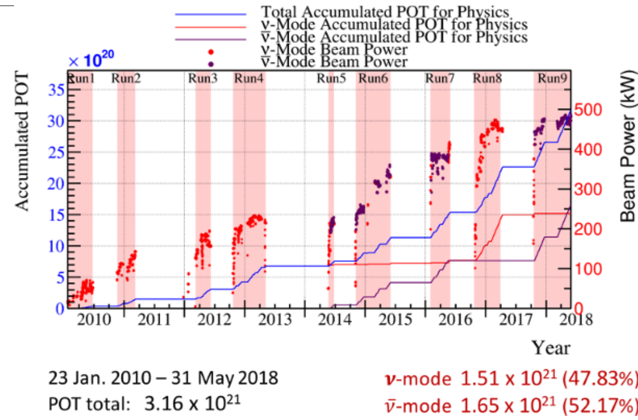

Figure 1.14: T2K accumulated protons on target since 2010 shows a steady increase in beam power over time. The gap between Run2 and Run3 is due to the damage suffered at J-PARC after the 2011 Tōhoku earthquake.

flux of neutrinos, a series of three current pulsed, focusing magnets called horns[9] as shown in Figure 1.12c on page 27 are used to focus the mesons of the correct charge towards SK. Photographs of a graphite target and focusing horn are shown in Figure 1.13 on page 27. The horns are pulsed at +250kA (-250kA) to select positively (negatively) charged pions. The focused pions are allowed to decay along the 96m long decay volume as to boost the daughter neutrinos along the secondary beamline direction. For safety reasons, the decay volume is filled with gaseous helium at 1 atm of pressure which has a low pion absorption rate. The daughter particles in the decay volume should be mostly muons and muon-neutrinos traveling towards SK. An beam dump is placed at the end of the decay volume to stop particles that have not yet decayed to prevent uncontrolled for decay products from contaminating the beam.

Along both beamlines are numerous monitors and timing systems to observe the proton beam to ensure stable production of neutrinos. Proton beam monitors are placed along the primary beamline to ensure the proton beam is properly steered into the secondary beamline. An optical transition radiation monitor is situated around the target to observe any protons not intersecting with the target region itself. The last monitor along the secondary beamline

[9] The name horn derives from the fact that the focusing magnets are shaped like brass horns in a music ensemble or marching band. One can think of these horns like a focusing lens for charged particles.

is the a muon monitor (MUMON), which is placed downstream of the beam dump to observe the daughter muons of > 5 GeV/c momentum [1].

In order to provide timing information for the neutrino beam at SK, a global positioning system (GPS) is used to synchronize clocks at SK and J-PARC. Any event outside the beam timing window are rejected in the T2K oscillation analysis, and so having precise timing information for the neutrino beam is critical for the experiment. The GPS has an internal accuracy of 50ns, or about $\sim$ 150m assuming the neutrinos are traveling near the speed of light. This is well within the time it takes for any neutrino to travel the 295 km between J-PARC and SK.

J-PARC continues to improve the proton delivery and neutrino modes since T2K begin in 2010. T2K has run in two horn current modes: ν-mode and $\overline{\nu}_\mu$-mode. Focusing positively charged pions with +250 kA horn current is called forward horn current (FHC) mode. Similarly, using -250 kA horn current is called reverse horn current (RHC) mode. The aggregate running of T2K for both FHC and RHC modes are shown in Figure 1.14 on page 28 in units of protons on target (POT).

In addition the proton beam intensity, as measured in kW (energy/proton/second), has been increased over time which increases the number of neutrino interactions observed at SK. Note that while $\pm$250 kA is the preferred horn current in both FHC and RHC modes, the horns were run briefly at +205kA when operations resumed after 2011 Tōhoku earthquake.

1.2.2 Neutrino Near Detectors: ND280

T2K has a near detector (ND) site at J-PARC that is designed specifically observe the neutrinos in flight. The purpose of a ND site is due to large uncertainties from the neutrino flux in previous neutrino oscillation experiments. The site is called ND280 and is located 280m away from the production target. The primary detector is an off-axis, magnetized tracking detector consisting of different subdetectors. A separate detector array called the Interactive Neutrino Grid (INGRID) measures the neutrino beam profile. Both on-axis and

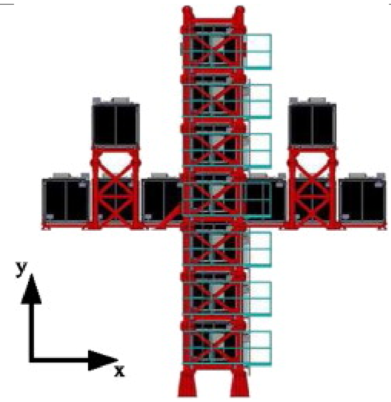

Figure 1.15: A schematic of INGRID shows the arrangement of the tracking scintillating modules. There are 16 identical modules total with seven in the vertical row, seven in the horizontal row, and two at off-axis positions. INGRID is capable of measuring the neutrino beam in a transverse area of 10m × 10 m. With the vertical row upstream of the horizontal row, the designed beam center intersects each row's center module [2].

off-axis detectors extensively utilize a commercial light sensor called a multi-pixel photon counter (MPPC) for the light collection in the scintillator-based detectors.

What follows from here is a description of the MPPC technology used in T2K. Next is a description of INGRID and its purpose at ND280. This is followed by a general description primary off-axis, magnetized detector. This subsection is finished with descriptions of two subdetectors in the off axis detector. The first and second being the pi-zero detector (PØD) and time projection chamber (TPC), respectively.

From here on unless specified, INGRID will refer only to the on-axis ND and ND280 will refer only to off-axis ND.

1.2.2.1 Multi-pixel photon counter (MPPC)

While the reliable photo-multiplier tube (PMT) technology was used in previous scintillator-based detectors, T2K needed a different technology to work in the strong magnetic field environment. T2K selected a commercially available silicon photomultiplier sensor developed by the Hamamatsu corporation called a MPPC. A MPPC is a compact device containing many sensitive avalanche photodiode pixels that act as Geiger micro-counters. They are well matched with the spectral emission of wavelength-shifting (WLS) fibers used to collect the

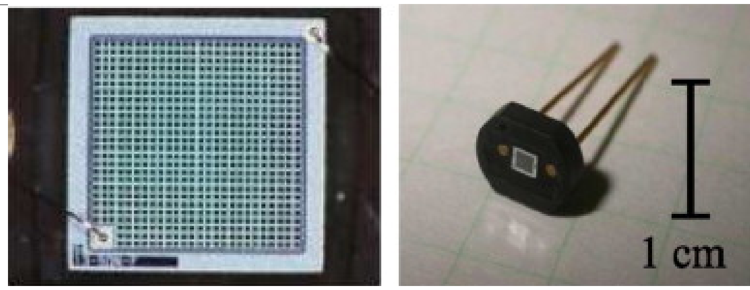

Figure 1.16: Photographs of the specially designed MPPC used in T2K. A magnified face view is shown on the left with an entire unit shown on the right [1].

scintillator light in ND280 and operate in a strong magnetic field environment. T2K utilizes specialized 667-pixel MPPCs with an effective area of 1.3 mm × 1.3 mm as shown in Figure 1.16 on page 31.

1.2.2.2 On-Axis Detector

The on-axis near detector called the Interactive Neutrino Grid (INGRID) is a tracking scintillator detector designed to directly measure the neutrino beam profile. As shown in Figure 1.15 on page 30, it is a cross grid of tracking modules centered at the designed neutrino beam center ($\theta = 0$). Each module consists of alternating layers of iron plates and scintillator bars except for the two most downstream scintillating layers which lack iron plates. To monitor the beam asymmetry, two separate modules are placed off the grid axis.

Each scintillating bar consists of scintillator-doped polystyrene which emits light when a charged particle deposits energy in the media. Each bar contains a single wavelength-shifting (WLS) fiber to collect and shift the light to a different energy. The light is collected at a single MPPC device and converted into an electrical signal. In order to enhance the collection efficiency, a reflective TiO_2 doped polystyrene shell surrounds each bar. Bars are assembled into planes to provide tracking capabilities. Veto planes also surround each module to prevent false signals to trigger.

INGRID is continually monitored to ensure the neutrino beam center is properly aligned at its designed center. Diagnostic plots such as Figure 1.17 on page 32 are collected on a

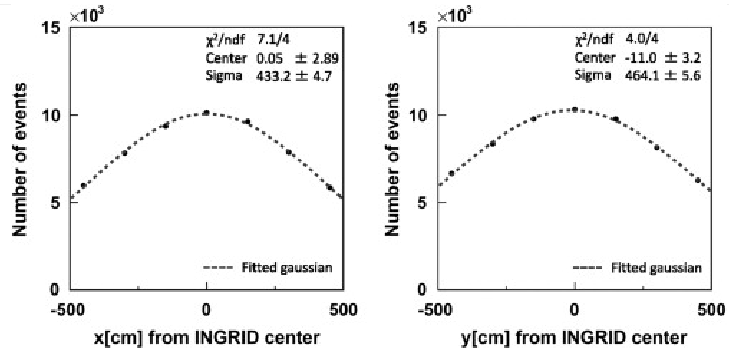

Figure 1.17: A beam profile taken with INGRID in April 2010 shows the Gaussian nature of the beam. The errors on the data points are about 1%. [2]

monthly basis to ensure that the neutrino flux at Super-Kamiokande (SK) is consistent with T2K's design. A history of the beam profile and event rate on INGRID between January 2010 and October 2016 is shown in Figure 1.18 on page 33.

1.2.2.3 Off-Axis Detector Summary

The primary near detector for T2K, ND280, is an off-axis, magnetized tracking detector. It is a collection of different detector technologies designed to facilitate three measurement goals:

1. ν_μ flux at SK,
2. Irreducible ν_e background flux at SK, and
3. ν_μ interaction backgrounds and cross sections for the $\nu_\mu \to \nu_e$ search.

ND280 consists of the pi-zero detector (PØD), the tracker region consisting of a fine grain detector (FGD) and time projection chamber (TPC), an electromagnetic calorimeter (ECal), and side muon range detector (SMRD). The ND280 subdetectors are instrumented inside the recycled UA1/NOMAD magnet with the SMRD in the magnetic field return yoke itself. A schematic of the different detector components of ND280 is shown in Figure 1.19 on page 34.

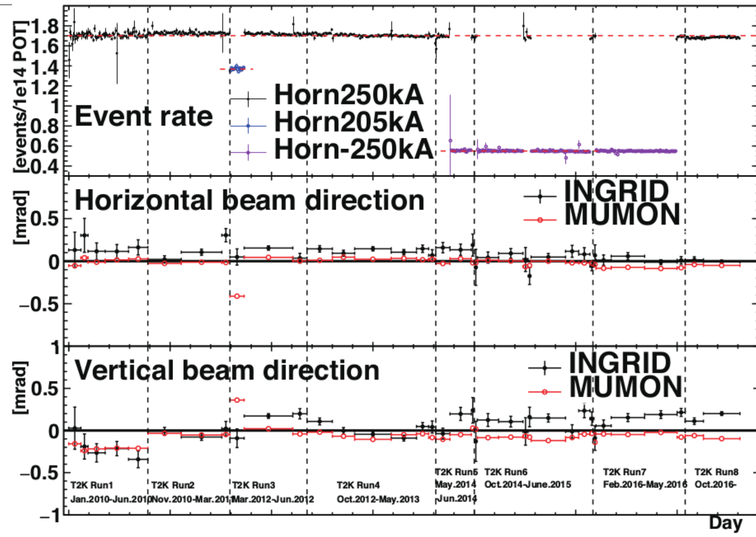

Figure 1.18: INGRID interaction event rate and beam profiles are shown. The top panel shows the event rate for the three different horn currents. The middle and bottom panels show the horizontal and vertical beam directions with respect to the beam center, respectively. A deviation of 1 mrad corresponds to a little under 30 cm. The error bars shown are the statistical errors on the mean.

The focus of this thesis are the PØD and the TPC since they are the primary subdetectors used in the analysis. The PØD serves as a massive target for the incident neutrino beam and the TPC serves to measure the charge and momentum of the outgoing particles.

The ND280 magnetic field is generated using electrical current fed through solenoid coils to generate a dipole field of strength 0.2 T[10] in the x direction. The field is highly uniform near the center of the detector which is where the majority of the TPC system is located. However, it has significant deviations from 0.2 T near the solenoid edges. In order to fully understand the field inside ND280, a precise 3D model was generated using a machine controlled Hall probe. The operating field strength during the mapping process was 0.07 T due to power restrictions at the time. The model was then compared with measurements in the TPC region as shown in Figure 1.20 on page 35. After scaling the model to the nominal

[10]This is a powerful magnetic field. According to the The US/UK World Magnetic Model for 2015-2020, the magnetic field strength on the surface of the Earth is about 0.294385 Gauss or 2.94385×10^{-5} T. So the field inside ND280 is about 6800 times more forceful than the Earth's influence [8].

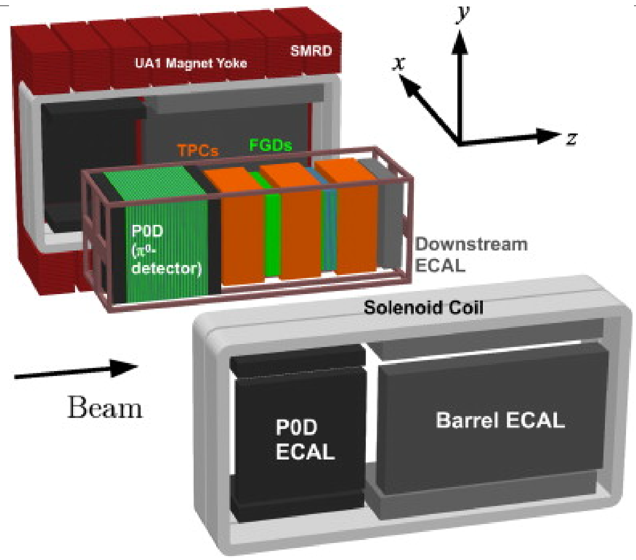

Figure 1.19: An exploded view of the ND280 off-axis detector. The magnetic field is generated from the Solenoid Coil via an electrical current which produces a dipole magnetic field of strength 0.2 T. The field is designed to return to the Magnetic Yoke.

operating strength of 0.2 T, a fractional uncertainty of 10^{-3} or uncertainty of 2 Gauss in each direction was obtained.

The ND280 magnetic field permits the measurements of particle charge and momentum. A particle of charge q, rest mass m_0, and velocity $\mathbf{v}$ under the influence of an external electric and magnetic fields, $\mathbf{E}$ and $\mathbf{B}$, respectively, experiences a force $\mathbf{F}$ given by the Lorentz force equation

$$\mathbf{F} = q\left(\mathbf{E} + \mathbf{v} \times \mathbf{B}\right). \tag{1.47}$$

Assuming for now that there is no external electric field, the force on the particle is

$$\mathbf{F} = q\mathbf{v} \times \mathbf{B}, \tag{1.48}$$

which is both orthogonal to $\mathbf{v}$ and $\mathbf{B}$. Since the mechanical work on a particle in a magnetic field is zero, the particle's energy is unchanged ($|\mathbf{v}| = v =$ constant). Newton's Second Law allows us to rewrite the force as an change in momentum $\mathbf{P}$

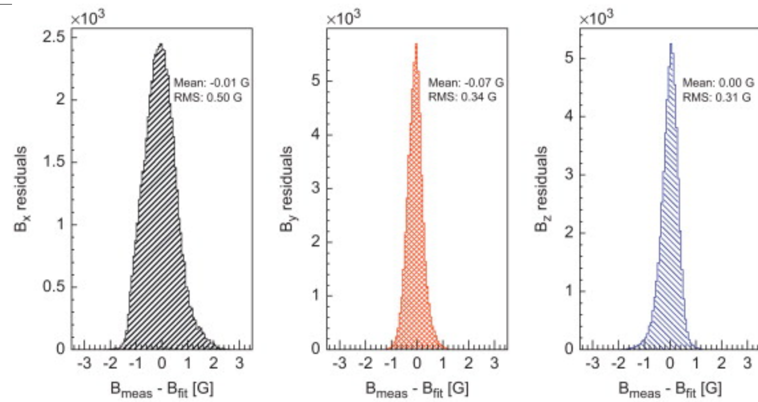

Figure 1.20: Each of the magnetic field components (x, y and z, respectively) are compared between a fit of the data and the actual measurements near the center of ND280. The systematic uncertainty on the field is extracted from the RMS of the mapping [1].

$$\begin{aligned}
\mathbf{F} &= \frac{d\mathbf{P}}{dt} \\
&= \frac{d}{dt}\left(\gamma(v) m_0 \mathbf{v}\right) \\
&= m_0 \mathbf{v}\left(\frac{d\gamma(v)}{dt}\right) + \gamma(v) m_0 \left(\frac{d\mathbf{v}}{dt}\right) \\
&= m_0 \mathbf{v}\left(\frac{d\gamma(v)}{dv}\right)\cancelto{0}{\left(\frac{dv}{dt}\right)} + \gamma(v) m_0 \mathbf{a} \\
&= \gamma(v) m_0 \mathbf{a},
\end{aligned} \tag{1.49}$$

where $\mathbf{P} = \gamma(v) m_0 \mathbf{v}$ is the relativistic momentum and $\gamma(v) = \left(1 - (v/c)^2\right)^{-1/2}$ is the Lorentz factor for relativistic particles. For uniform circular motion, the magnitude of the acceleration is given by

$$|\mathbf{a}| = v^2/R \tag{1.50}$$

where R is the radius of curvature for the circle. Combining (1.50) and (1.49) with some algebra yields

$$R = \frac{\gamma(v) m_0 v}{q\,|\mathbf{B}|\sin\theta_{\mathbf{vB}}}, \tag{1.51}$$

where $\theta_{\mathbf{vB}}$ is the angle between $\mathbf{v}$ and $\mathbf{B}$. The numerator of (1.51) is recognized as the magnitude of the momentum $|\mathbf{P}|$. Some further rearrangement yields

$$|\mathbf{P}| = q\,|\mathbf{B}|\,R\sin\theta_{\mathbf{vB}}, \tag{1.52}$$

and thus measuring the direction and radius of curvature inside the field provides the charge and momentum, respectively, as desired.

1.2.2.4 Off Axis Pi-zero detector (PØD)

1.2.3 Neutrino Far Detector: Super-Kamiokande

1.2.3.1 Oscillation Analysis

The number of reconstructed neutrino events of flavor α observed at SK is sum of all true charged current (CC) events $S^{\mathrm{FD}}_{\nu_\alpha}$ and backgrounds B

$$N^{\mathrm{SK}}_{\nu_\alpha} = S^{\mathrm{SK}}_{\nu_\alpha} + B$$

where

$$\begin{gathered} S^{\mathrm{SK}}_{\nu_\alpha} = \sum_i \sum_\beta \sum_m \mathcal{P}_{\nu_\beta \to \nu_\alpha}\left(E_{\nu,i};\vec{o}\right) \times \sigma^m_{\nu_\alpha}\left(E_{\nu,i}\right) \\ \times\, \Phi^{\mathrm{SK}}_{\nu_\alpha}\left(E_{\nu,i}\right) \times T^{\mathrm{SK}} \times \epsilon^{\mathrm{SK}}\left(p_\alpha,\theta_\alpha\right) \end{gathered},$$

Bibliography

[1] K. Abe et al. The T2K Experiment. *Nucl. Instrum. Meth.*, A659:106–135, 2011. 23, 26, 27, 29, 31, 35

[2] K. Abe et al. Measurements of the T2K neutrino beam properties using the INGRID on-axis near detector. *Nucl. Instrum. Meth.*, A694:211 – 223, 2012. 30, 32

[3] K. Abe et al. Observation of Electron Neutrino Appearance in a Muon Neutrino Beam. *Phys. Rev. Lett.*, 112:061802, 2014. 24

[4] K. Abe et al. Search for CP Violation in Neutrino and Antineutrino Oscillations by the T2K Experiment with 2.2×10^{21} Protons on Target. *Phys. Rev. Lett.*, 121:171802, Oct 2018. 24

[5] C. Adams et al. The Long-Baseline Neutrino Experiment: Exploring Fundamental Symmetries of the Universe. 2013. arXiv:1307.7335. 4, 19, 23

[6] Jiro Arafune, Masafumi Koike, and Joe Sato. CP violation and matter effect in long baseline neutrino oscillation experiments. *Phys. Rev. D*, 56:3093–3099, Sep 1997. 22

[7] J-PARC Center. What is J-PARC?, January 2019. https://j-parc.jp/researcher/en/about/what/index.html, Accessed on 26 January 2019. 25

[8] A. Chulliat and Others. The US/UK World Magnetic Model for 2015-2020. Technical report, National Geophysical Data Center, NOAA, 2015. 33

[9] A. de Gouvea et al. Working Group Report: Neutrinos. In *Proceedings, 2013 Community Summer Study on the Future of U.S. Particle Physics: Snowmass on the Mississippi*, 2013. arXiv:1310.4340. 19

[10] I. Esteban et al. Global analysis of three-flavour neutrino oscillations: synergies and tensions in the determination of $\theta_{23}, \delta_{\text{CP}}$, and the mass ordering. 2018. arXiv:1811.05487. 21

[11] A. Ferrero. The ND280 Near Detector of the T2K Experiment. *AIP Conference Proceedings*, 1189(1):77–82, 2009. 23

[12] S. Fukuda et al. The Super-Kamiokande detector. *Nuclear Instruments and Methods in Physics Research Section A: Accelerators, Spectrometers, Detectors and Associated Equipment*, 501(2):418 – 462, 2003. 23

[13] Susumu Igarashi. Recent Progress of J-PARC MR Beam Commissioning and Operation. In *Proceedings, 57th ICFA Advanced Beam Dynamics Workshop on High-Intensity and High-Brightness Hadron Beams (HB2016): Malmö, Sweden, July 3-8, 2016*, page MOAM6P60, 2016. 26

[14] C. Jarlskog. A Basis Independent Formulation of the Connection Between Quark Mass Matrices, CP Violation and Experiment,. *Z. Phys.*, C29:491–497, 1985. 20

[15] E. Komatsu and Others. Seven-year Wilkinson Microwave Anisotropy Probe (WMAP) Observations: Cosmological Interpretation. *Astrophys. J.*, 192:18, February 2011. 22

[16] Z Maki, M. Nakagawa, and S. Sakata. Remarks on the Unified Model of Elementary Particles. *Progr. Theor. Exp. Phys.*, 28(5), 1962. 17

[17] B. Pontecorvo. Inverse Beta Processes and Nonconservation of Lepton Charge. *J. Exp. Theor. Phys.*, 28(5), 1957. 17

[18] P. K. Saha et al. Simulation, measurement, and mitigation of beam instability caused by the kicker impedance in the 3-GeV rapid cycling synchrotron at the Japan Proton Accelerator Research Complex. *Phys. Rev. Accel. Beams*, 21:024203, Feb 2018. 26

[19] Andrei D Sakharov. Violation of CP invariance, C asymmetry, and baryon asymmetry of the universe. *Soviet Physics Uspekhi*, 34(5):392, 1991. 23

[20] N. Schmitz. *Neutrinophysik*. Teubner, Stuttgart, 1997. 16

[21] T. Sekiguchi et al. Development and operational experience of magnetic horn system for T2K experiment. *Nuclear Instruments and Methods in Physics Research Section A: Accelerators, Spectrometers, Detectors and Associated Equipment*, 789:57 – 80, 2015. 27

[22] M. Tanabashi et al. The Review of Particle Physics. *Phys. Rev. D*, 98(030001), 2018. 17, 21

[23] Peter von Ballmoos. Antimatter in the Universe: constraints from gamma-ray astronomy. *Hyperfine Interactions*, 228(1):91–100, Oct 2014. 22

[24] Y. Yamazaki, editor. *Accelerator technical design report for high-intensity proton accelerator facility project, J-PARC*. Number 2002-013. Japan Atomic Energy Research Institute, 2003. 26

[25] Kai Zuber. *Neutrino Physics*. CRC Press, Boca Raton, FL., 2nd edition, 2012. 2, 11, 16